Strangeness Enhancement in Fixed-Target Pb-Ne Collisions with LHCb SMOG Experiment

Federica Fabiano, federica.fabiano96@gmail.com
Supervisors: Dr. Pasquale Di Nezza, Dr. Marco Santimaria

CERN Summer Student Programme 2021

Abstract. At sufficiently high temperature and energy density, nuclear matter converts to a phase where quarks and gluons are not confined: the Quark-Gluon Plasma (QGP). Such a state is produced in the laboratory with ultra-relativistic collisions of heavy nuclei, resulting in an enhanced strange hadrons' production. Strangeness enhancement has been proposed as a test of the Quark-Gluon Plasma formation due to: (i) the dominance of the $gg \to s\bar{s}$ channel and (ii) the high gluon and high strange quark densities in QGP. Here I report on the analysis of the samples related to fixed-target Pb-Ne and p-Ne collisions at $\sqrt{s_{NN}} = 68.6$ GeV collected with SMOG at LHCb.

1 Introduction

LHCb is the only experiment among all LHC experiments that can take data both in collider and fixed-target mode. The LHCb fixed-target system, called SMOG (System for Measuring the Overlap with Gas), allows to inject a low flow rate of noble gas into the vacuum vessel of the LHCb vertex detector (VELO) [1,2]. Albeit it was originally conceived for luminosity measurements, the SMOG system gives the opportunity to study proton-nucleus and nucleus-nucleus collisions on various target types and at different center-of-mass energies. During LHC Run-3, the new system SMOG2 will be put in operation with a new storage cell that will allow more efficient beam-gas collisions and several new measurements.

The main physics search of this report is the Quark Gluon Plasma (QGP) formation in Lead-nucleus collisions, resulting in an enhanced strange hadrons' production. Indeed, since QGP is characterized by a dominance of the $gg \to s\bar{s}$ channel and high gluon and high strange quark densities, the strangeness enhancement has been proposed as the signature of this strongly-interacting QCD (Quantum Chromo-Dynamics) matter's formation.

The first part of the work will focus on the data analysis of non-strange hadrons, such as protons and pions: a sample comparison between pA and PbA data will provide further information on their behaviour. Then, this information will be useful for the strange-hadron data normalization. Indeed, our measurement focuses on the double-strange meson ϕ production in Pb-Ne (where QGP is most likely to origin) and p-Ne (where QGP will not arise) collisions.
After applying custom analysis cuts on both samples, a fit will be performed to the ϕ invariant mass over the entire transverse momentum range and when dividing the latter in bins with equal integral.

1.1 Strangeness Production with SMOG

As previously anticipated, our measurement focuses on the double-strange meson ϕ production in both PbA and pA collisions. However, this report will also highlight the role protons and pions play in the analysis scene.
The full strangeness production with SMOG comprehends:

- non-strange hadrons $\pi^{\pm}$, p, $\bar{p}$;
- single-strange mesons $K^{\pm}, K^0_S$;
- single-strange baryons $\Lambda, \bar{\Lambda}$;
- double-strange meson ϕ;
- double-strange baryons $\Xi^-, \bar{\Xi}^+$;
- triple-strange baryons $\Omega^-, \bar{\Omega}^+$.

The dominant decay modes of these strange hadrons with their branching ratios are listed below:

- $K_S^0 \to \pi^+\pi^-$ BR = 69.2%;
- $\Lambda \to p\pi$ BR = 63.9%;
- $\phi \to K^+K^-$ BR = 49.2%;
- $\Xi \to \Lambda\pi$ BR = 99.9%;
- $\Omega \to \Lambda K$ BR = 67.8%.

In this analysis, protons, pions and the ϕ meson will be fully studied by comparing data from Pb-Ne and p-Ne collisions. These two samples will be introduced in the next section.

2 Samples and Analysis Cuts

The main purpose of this analysis is the search for QGP formation (Figure 1) through a strangeness enhancement in heavy-ion collisions with the noble gas. Heavy quarks are effective probes to study the properties of a de-confined medium such as QGP, indeed:

- their masses are significantly higher than the QGP critical temperature ($T_C \sim 156$ MeV);
- they are produced in the early stages of the collision in a timescale shorter than the QGP formation;
- their overall yields are not modified by the medium, but the latter is expected to affect the formation of hidden heavy-flavour bound states. This feature is the key for QGP formation.

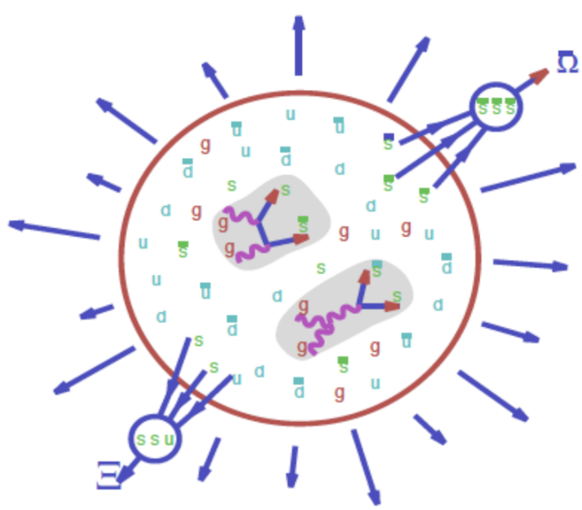

Fig. 1. Quark-Gluon Plasma content.

2.1 Samples Comparison

Among all the data collected with SMOG, the samples considered in this analysis are from proton-Neon (small system) and Lead-Neon (large system) collisions at the same center-of-mass energy $\sqrt{s_{NN}} = 68.6$ GeV [3]:

- the 2017 p-Ne data have been collected in parallel of high intensity pp collisions with 2.5 TeV proton beams ($L \sim 200\text{nb}^{-1}$);
- the 2018 Pb-Ne data have been collected in parallel of Pb-Pb collisions with 2.5 TeV/nucleon Pb beams ($L \sim 0.3\text{nb}^{-1}$).

Figure 2 shows all the SMOG collected data through the years and with different noble gases [4]. The two highlighted columns refer to the considered samples.

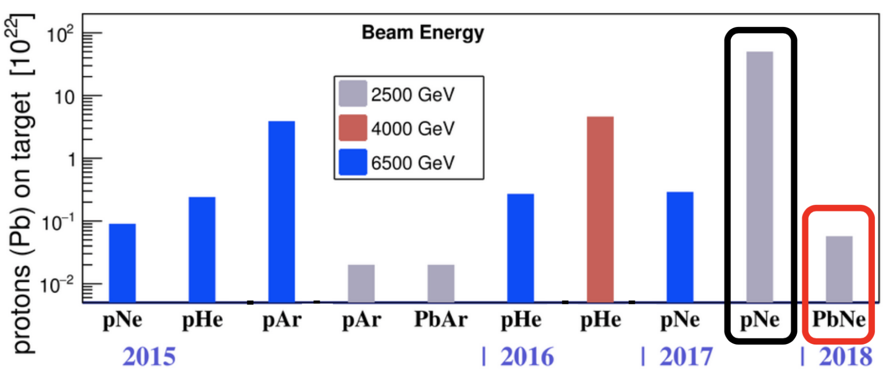

Fig. 2. SMOG data collected through the years and with different noble gases. The two highlighted columns refer to the samples considered in this analysis.

2.2 Global Cuts

Before proceeding with the comparison, custom analysis cuts (called ”global cuts”) have been performed on both samples to ensure the correct interaction type and the goodness of the reconstructed tracks. Indeed, the variables selected for this purpose refer to the tracks' topology and the bunch crossing type. The selection procedure each sample underwent to is listed and explained in the following [3]:

- **BCType==1** to avoid beam ghost-charge contamination due to proton-proton collisions;
- **nPVs>=1** to guarantee at least one Primary Vertex (PV) found;
- **nBackTracks<5** that is the number of VELO Tracks going backward;
- **nLongTracks>0** that is the number of tracks with a hit in all detectors;

- **PVNTRACKS[0]>=5** to guarantee that at least 5 tracks belong to the Primary Vertex;
- **PVNTRACKS[0]>PVNTRACKS[i]** with i>0;
- **_ProbNNp(pi)>0.5** to ensure the presence of produced protons (pions);
- **-700<PVZ[0]<200** && **PVZ[0]<-100** || **PVZ[0]>100** to avoid ghost-event PVs from *pp* collisions;
- **Hit1BEMicroBiasVeloDecision_Dec** that is the trigger condition.

At the end of the selection, the considered samples can be compared through a set of variables that comprehends: rapidity y and pseudorapidity η, momentum P and its transverse component P_T, and the number of tracks in an event N_{tracks} and the number of scintillator hits before the VELO $nSPDHits$.

The results will be presented in the next paragraph for the produced protons, pions and ϕ, i.e. two non-strange hadrons and a double-strange meson respectively.

3 Analysis Results

The results obtained in two months of Summer School will be presented in this section, together with the open issues of the analysis procedure.

3.1 Non-Strange Hadrons: Protons and Pions

As previously anticipated, after applying all the cuts in 2.2, the two samples have been compared through the following sets of variables:

- rapidity y and pseudorapidity η;
- particle momentum P and its transverse component P_T;
- multiplicity N_{tracks} and scintillator hits before the VELO $nSPDHits$.

Figure 3 reports the analysis for produced protons, while Figure 4 shows the results for pions. All distributions have been normalized to 1.

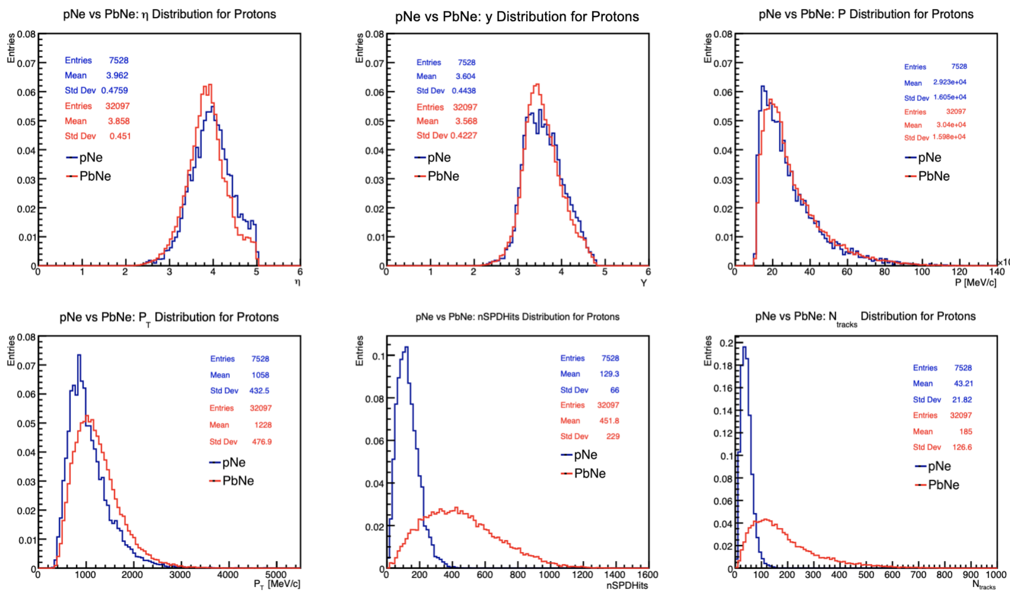

Fig. 3. Results for protons after applying the global cuts to p-Ne (blue) and Pb-Ne (red) samples.

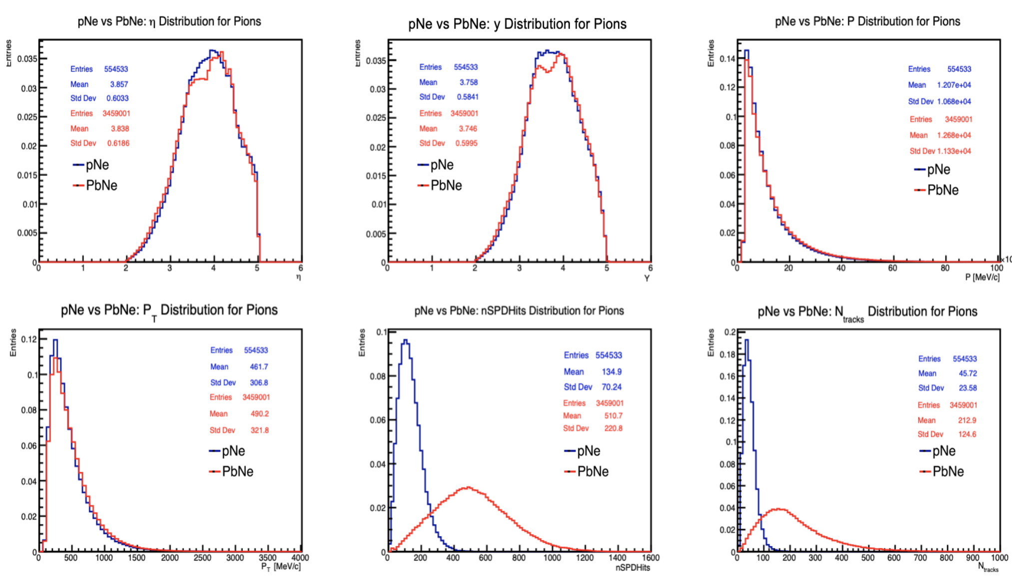

Fig. 4. Results for pions after applying the global cuts to p-Ne (blue) and Pb-Ne (red) samples.

While protons behave regularly through all the considered variables and for the two samples, pions show some irregularities in rapidity and pseudorapidity for Pb-Ne sample: indeed, two peaks can be appreciated in the latter figure (Figure 4). However, the other distributions for pions do not present any difference in shape, as expected for a non-strange particle which behave equally both in cold (p-Ne) and hot (Pb-Ne) nuclear matter.
We have investigated the origin of the non-coincidence of the two samples in η for pions by exploring at first η as a function of the z-coordinate of the primary vertex PVZ[0] for Pb-Ne with (b) and without (a) the PVZ[0]<-100 || PVZ[0]>100 cut (Figure 5), and then by re-arranging the analysis in two different PVZ[0] regions with the further condition on PVX and PVY, $\sqrt{PVX[0]^2 + PVY[0]^2} < 3$ mm, as Figure 6 reports.

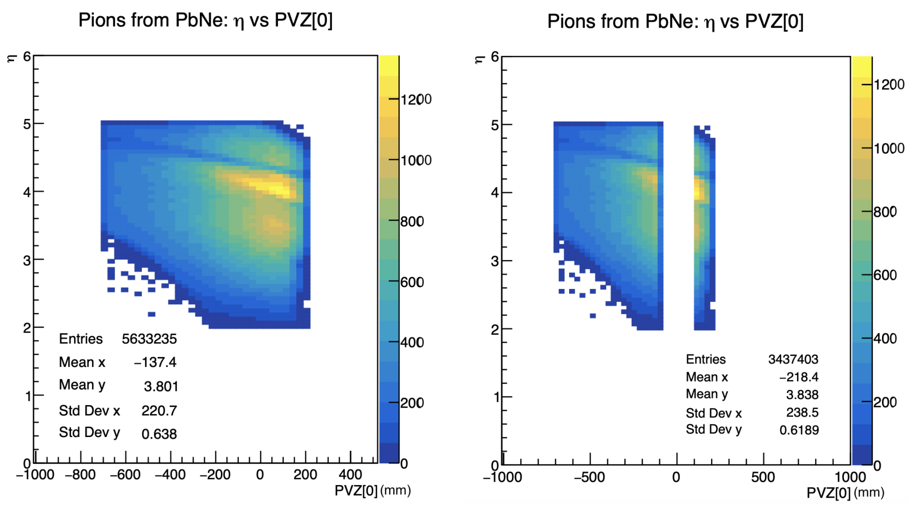

(a) Without PVZ(0)<-100 || PVZ(0)>100 cut.

(b) With PVZ(0)<-100 || PVZ(0)>100 cut.

Fig. 5. η as a function of the z-coordinate of the primary vertex PVZ(0) for Pb-Ne sample in two different cases.

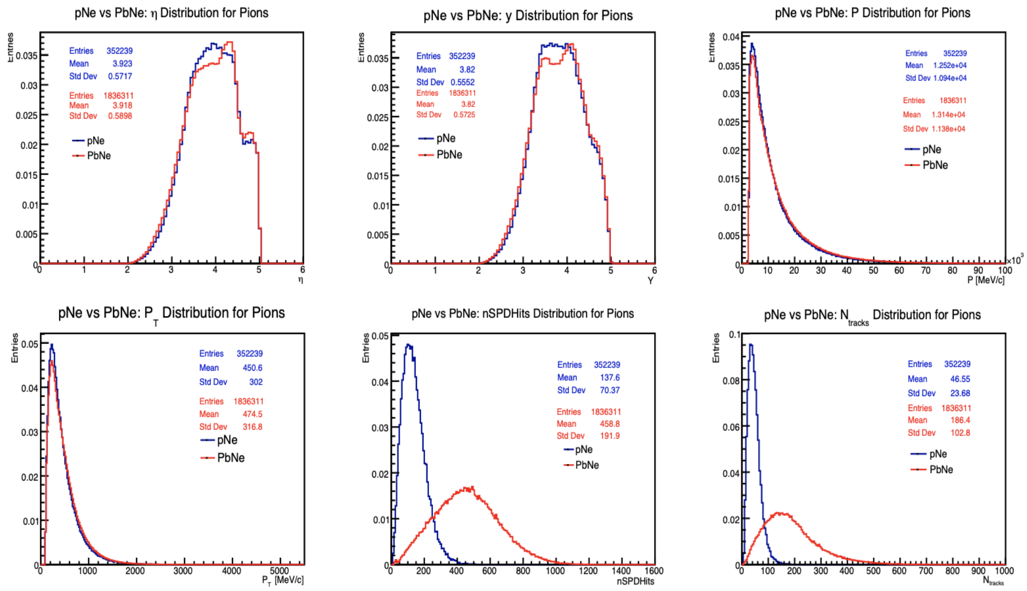

(a) -700 < PVZ(0) (mm) < -200.

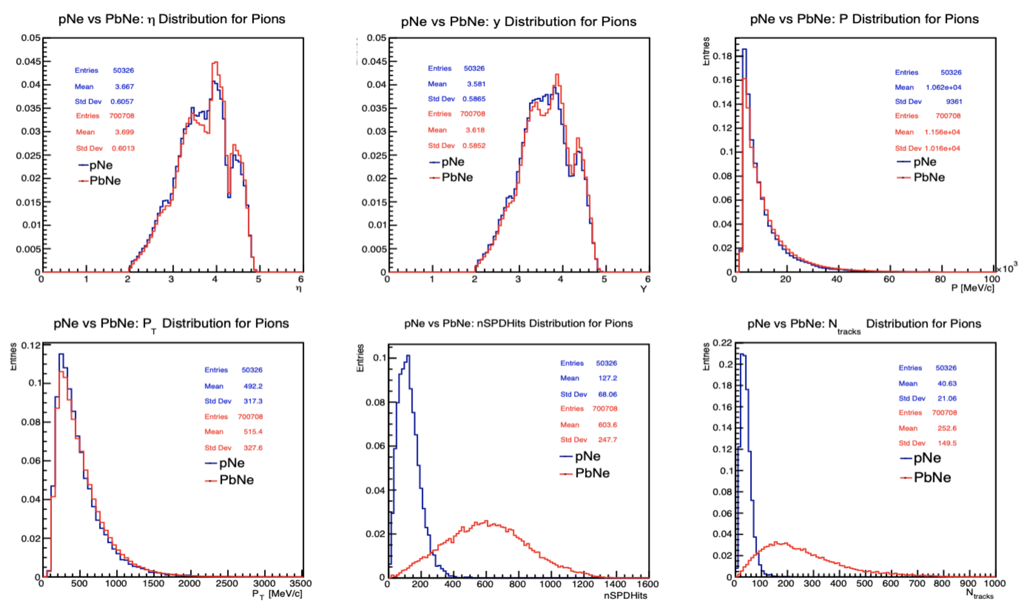

(b) 100 < PVZ(0) (mm) < 200.

Fig. 6. Pions for both p-Ne (blue) and Pb-Ne (red) samples in two different PVZ(0) regions, with the further condition $\sqrt{PVX[0]^2 + PVY[0]^2} < 3$ mm applied.

We have thus decided to exclude the central region PVZ[0] (mm) $\in [-100, 100]$ to avoid ghost tracks from pp collisions, but further studies are needed to fully understand the two peaks in Pb-Ne rapidity and pseudorapidity for pions.

3.2 Double-Strange Meson: ϕ

This section is dedicated to the reconstruction and fit on the ϕ invariant mass over the entire transverse momentum P_T range, and when dividing the P_T spectrum in bins with equal content. Then, the RooFit result will be checked with the sPlot procedure [5]. In order to perform a good fit, in addition to global cuts, PID cuts must be considered. However, the cuts for this hadron are different from the ones in Section 2.2 and listed below:

- BCType==1;
- nPVs>=1;
- PVNTRACKS[0]>=5 (>=14 for Pb-Ne)
- PVNTRACKS[0]>PVNTRACKS[i] with i>0;
- nLongTracks>0;
- PVZ[0]>=-700 && PVZ[0]<=-100 && nBackTracks<5) || (PVZ[0]>=100 && PVZ[0]<=200 && Loki_PUHits<5)
  Loki_PUHits<=10 for Pb-Ne;

The PID cuts instead concern mainly the decay kinematics of the ϕ meson, i.e. $\phi \to K^+K^-$ (Section 1.1):

- phi_1020_MAXDOCACHI2<=10 (Pb-Ne);
- phi_1020_ENDVERTEX_CHI2<9;
- phi_1020_IPCHI2_OWNPV<9;
- Kplus_TRACK_GhostProb<0.3 && Kminus_TRACK_GhostProb<0.3;
- Kplus_ETA>1.9 && Kplus_ETA<4.5 && Kminus_ETA>1.9 && Kminus_ETA<4.5;
- Kplus_TRACK_CHI2NDOF<3 && Kminus_TRACK_CHI2NDOF<3;
- Kplus_TRACK_Type==3 && Kminus_TRACK_Type==3;
- Kplus_IPCHI2_OWNPV<9 && Kminus_IPCHI2_OWNPV<9;
- Kplus_ProbNNk>0.2 && Kminus_ProbNNk>0.2.

After applying these cuts, the fit to ϕ invariant mass can be performed: a convolution of a Breit-Wigner and a Gaussian is used for the signal (with free parameters), while a 1^{st} degree Chebyshev polynomial is considered for the background. The resulting fit in the total P_T range $0 < P_T$ (MeV/C)$< 14,000$ is reported in Figure 7 for both samples. On the top-left part of the plot, signal and background yields are reported. While the p-Ne sample is not overwhelmed by the background, the Pb-Ne one must undergo other selection cuts to further enhance the signal contribution.

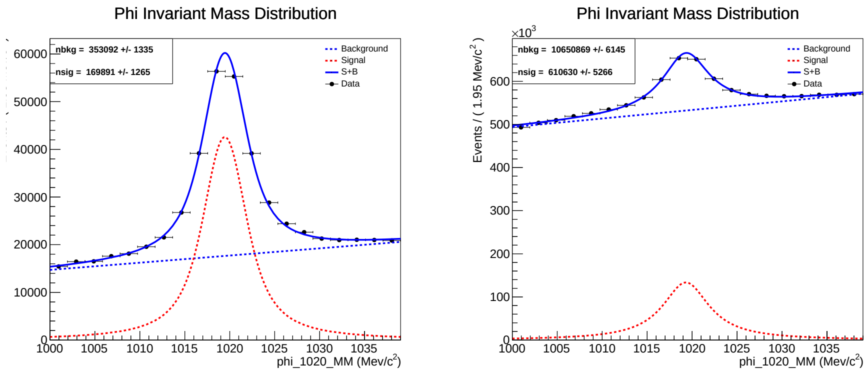

(a) p-Ne sample.

(b) Pb-Ne sample.

Fig. 7. Fit to the ϕ invariant mass for $0 < P_T$ (MeV/C)$< 14,000$ for the two samples. Blue Dashed Line: 1^{st} degree Chebyshev polynomial (background); Red Dashed Line: Breit-Wigner convoluted with a Gaussian (signal); Blue Solid Line: Signal + Background; Black Dots: Data.

This procedure has been repeated by dividing the P_T distribution at first by 99 bins with equal integral and then by 48 bins. Each one of them has been fitted with the previous model, but considering fixed parameters for the Breit-Wigner distribution. Figure 8 presents 4 out of 48 fits to show that the performed fits are good in all 48 bins, even at low momentum. They refer to the p-Ne sample where a ProbNNk>0.2 cut is applied. The 99 fits can be found at `https://cernbox.cern.ch/index.php/s/10963F3ZWhDW0QP`, while the 48 ones at `https://cernbox.cern.ch/index.php/s/TtvgE4E9dL5g0HY`.

In order to further reduce the background contribution for this sample, a more stringent cut has been applied: ProbNNk>0.7. Figure 9 reports the resulting fits in the same bins of Figure 8. The background yield is indeed decreased: the signal over background ratio in the central bin 962< P_T (MeV/C)<986 has improved from S/B = (48.7±0.5)% with the ProbNNk>0.2 cut to S/B = (67.4±1.2)% with ProbNNk>0.7. More cuts needed to further increase this value. All the fits for 48 bins in this configuration can be found at `https://cernbox.cern.ch/index.php/s/C6tVudRY6zOmvZU`.

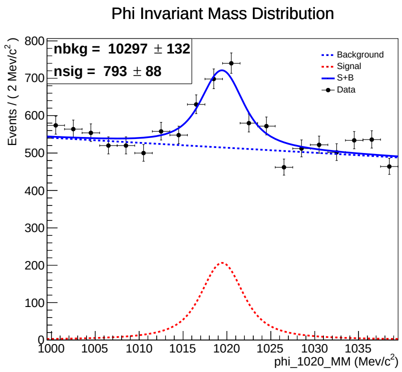

(a) 350 <P_T(MeV/c)< 408.

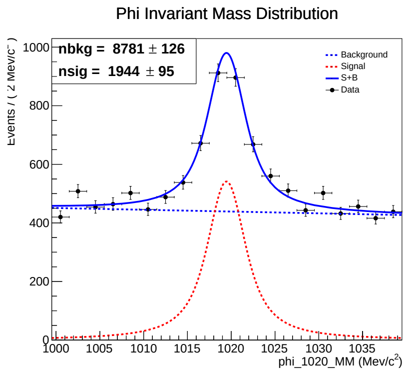

(b) 562 <P_T(MeV/c)< 584.

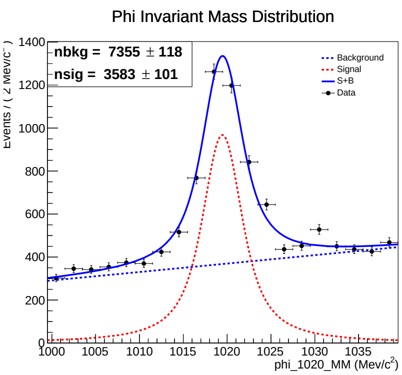

(c) 962 <P_T(MeV/c)< 584.

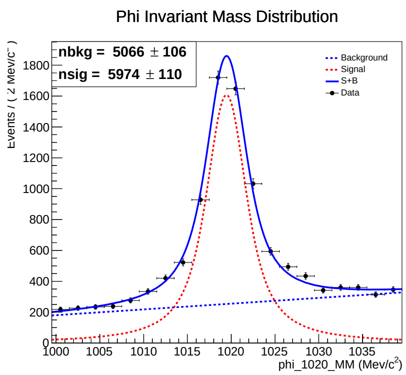

(d) 2006 <P_T(MeV/c)< 2302.

Fig. 8. p-Ne sample with ProbNNk>0.2 cut: fit to the ϕ invariant mass for different P_T bins. Blue Dashed Line: 1^{st} degree Chebyshev polynomial (background); Red Dashed Line: Breit-Wigner convoluted with a Gaussian (signal); Blue Solid Line: Signal + Background; Black Dots: Data.

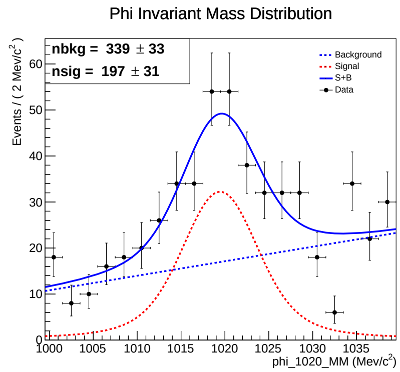

(a) 350 < P_T (MeV/c)< 408.

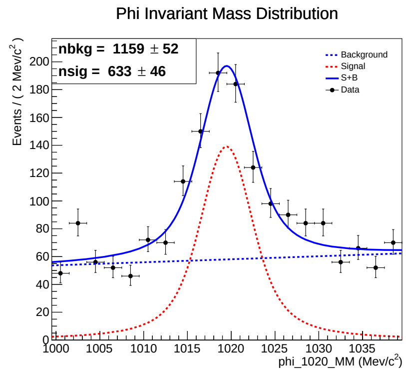

(b) 562 < P_T (MeV/c)< 584.

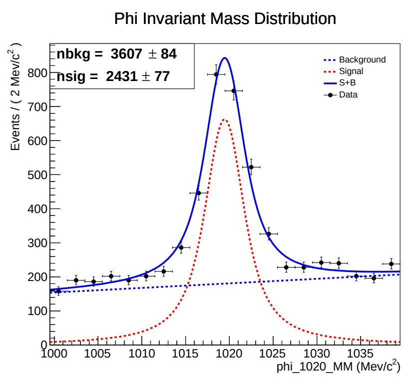

(c) 962 < P_T (MeV/c)< 584.

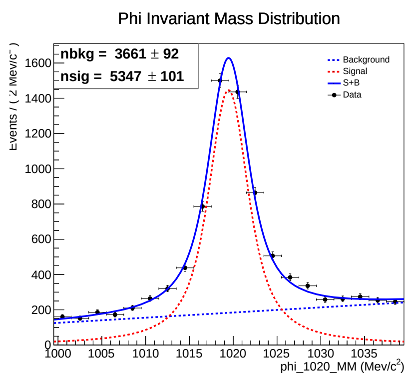

(d) 2006 < P_T (MeV/c)< 2302.

Fig. 9. p-Ne sample with ProbNNk>0.7 cut: fit to the ϕ invariant mass for different P_T bins. Blue Dashed Line: 1^{st} degree Chebyshev polynomial (background); Red Dashed Line: Breit-Wigner convoluted with a Gaussian (signal); Blue Solid Line: Signal + Background; Black Dots: Data.

The same procedure has been applied to the Pb-Ne sample, but choosing as background model a 2^{nd} degree Chebyshev polynomial. The resulting 48 fits with the ProbNNk>0.2 cut can be found at this link `https://cernbox.cern.ch/index.php/s/uolB8vybqqa4Peg`, while the others with ProbNNK>0.7 at `https://cernbox.cern.ch/index.php/s/HZl2GJW8kIyLlmK`.

The signal yields for the two configurations, i.e. the p-Ne sample with the two ProbNNk cuts applied, has been evaluated as a function of P_T bins (Figure 10). As expected, the more prohibitive cut ProbNNk>0.7 eliminates more background.

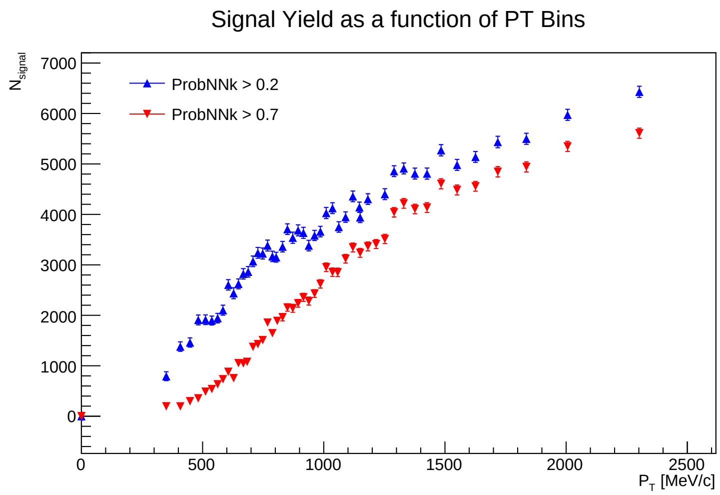

Fig. 10. Signal yields for the p-Ne sample in two different configurations: ProbNNK>0.2 (blue); ProbNNK>0.7 (red).

This trend will be compared to the sPlot result. For this purpose, the correlation between the ϕ invariant mass M_ϕ and its transverse momentum P_T must be controlled. Figure 11 reports the correlation between these two latter quantities for the two samples: p-Ne and Pb-Ne. While for the first one the correlation factor is 0.026, for Pb-Ne the value amounts to 0.058.

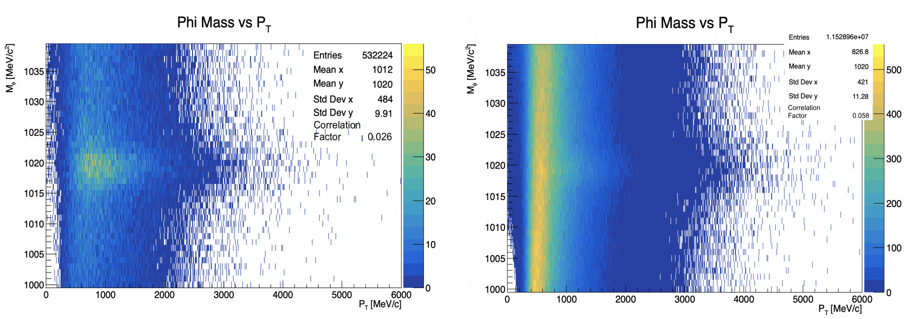

(a) p-Ne. (b) Pb-Ne.

Fig. 11. Correlation between M_ϕ and P_T for the two samples.

Given these two correlation factors, the sPlot check can be performed for the two samples. Indeed, it is necessary for the variables M_ϕ and P_T to be uncorrelated to perform the sPlot procedure.

3.2.1 sPlot Results This paragraph is dedicated to the results obtained until the moment of writing for the sPlot check of the two considered samples.
Figure 12 highlights the difference between the initial P_T distribution and the final one weighted with the sPlot signal sWeights for the two samples with ProbNNK>0.2. Both distributions have been normalized to 1. The configuration with the ProbNNK>0.7 cut is still under investigation, thus it is not reported here.

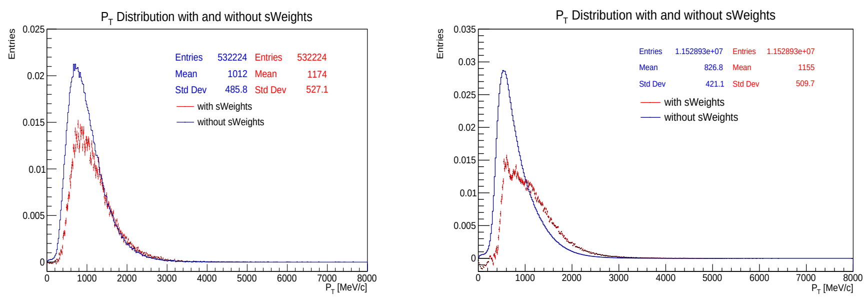

(a) p-Ne. (b) Pb-Ne.

Fig. 12. P_T distribution with (red) and without (blue) the sPlot signal sWeights for the two samples and ProbNNK>0.2.

As expected, the weighted distribution is different from the initial one: to appreciate how the sWeights work as a function of P_T, their correlation is reported in Figure 13.

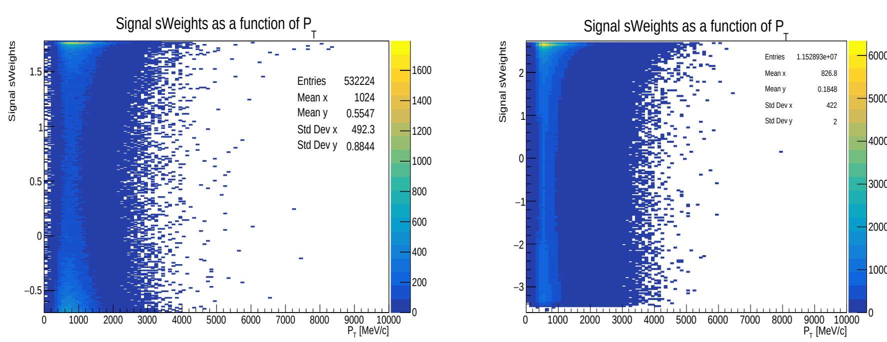

(a) p-Ne. (b) Pb-Ne.

Fig. 13. sPlot signal sWeights as a function of P_T for the two samples with ProbNNK>0.2.

4 Conclusion

The two samples studied in this work, i.e. p-Ne and Pb-Ne, have been completed, but their selection cuts are still under investigation.

The first part was dedicated to the study of non-strange hadrons, such as protons and pions. We have found anomalies in the rapidity and pseudorapidity distribution for the Pb-Ne sample: two peaks have been investigated with stringent selection cuts on the z-coordinate of the primary vertex, but more selection is needed to fully understand their origin.

The second part focused on the double-strange meson ϕ. We have performed a fit on its invariant mass (M_ϕ) over the entire P_T range, modelling the shape with a convolution of a Breit-Wigner with a Gaussian for the signal and a 1^{st} degree Chebyshev polynomial for the background.
Furthermore, good statistics for M_ϕ fit has been reached by dividing the P_T range in 99 and then 48 bins with equal integral. The bin number could be easily changed in the implemented code.
For the M_ϕ fit other models have been tested, such as 2 Gaussians, 2 Crystal Ball for signal and 2^{nd} degree Chebyshev polynomial for background. However, the final choice (Breit-Wigner $\times$ Gauss) guaranteed a good fit both for all P_T range and for binned P_T, and the two PID cuts configurations.

Since the correlation between M_ϕ and P_T amounted to 0.026 (0.058) for p-Ne (Pb-Ne), the sPlot check could be performed finding a re-defined shape of the transverse momentum distribution for the two samples.

In order to finish the comparison, three more steps must be accomplished: (i) the signal yield as a function of the transverse momentum must be checked with the sPlot result for the two ProbNNk cuts; (ii) the same binning procedure carried out for the variables M_ϕ, P_T will be repeated for multiplicity using "nVeloTracks"; (iii) finally, a ratio between p-Ne and Pb-Ne samples will be studied as a function of the observables $y, \eta, P, P_T, N_{tracks}$ and $nSPDHits$.

5 Acknowledgements

I am grateful to my supervisors Pasquale and Marco for helping and supporting me in every step of the way going through with this interesting project, and to CERN for giving this unforgettable opportunity to participate in the Summer Student Programme.

References

1. C. Barschel, *Precision Luminosity Measurement at LHCb with Beam-Gas Imaging*, PhD thesis, RWTH Aachen U. (2014).
2. R. Aaij et al., *Performance of the LHCb Vertex Locator*, JINST 9 (2014) P09007, arXiv:1405.7808.
3. F. Fleuret et al., *Global Event Cuts for 2017 pNe SMOG Data*, `https://cds.cern.ch/record/2720461/files/LHCb-INT-2020-012.pdf`
4. The LHCb Collaboration, *LHCb SMOG Upgrade*, `https://cds.cern.ch/record/2673690/files/LHCB-TDR-020.pdf`
5. M Pivk and F.R. Le Diberder, *sPlot: a Statistical Tool to Unfold Data Distributions*, arXiv:physics/0402083v3 [physics.data-an] 2 Sep 2005.